



Cite this: *Green Chem.*, 2015, **17**, 2912

The effect of steam on the catalytic fast pyrolysis of cellulose

H. Yang,^{a,b} R. J. Coolman,^b P. Karanjkar,^b H. Wang,^b Z. Xu,^b H. Chen,^a T. J. Moutziaris^c and G. W. Huber^{*b}

The effect of steam for the catalytic fast pyrolysis of cellulose with ZSM-5 was studied in a bubbling fluidized bed reactor. Irreversible and reversible changes due to steaming were identified. Steam caused dealumination, a loss of total acidity, an increase in the zeolite-crystal size, and agglomeration of particles. For runs both with and without steam co-feeding, these irreversible changes caused lower yields for aromatics and char/coke, and higher yields for methane and unidentified products. In addition to irreversible catalyst changes, steam co-feeding was also found to reversibly lower yields of aromatics, char/coke, and identifiable oxygenate species, increase yields of CO and methane, and not change the overall yields of CO₂ and olefins.

Received 5th January 2015,
Accepted 9th March 2015

DOI: 10.1039/c5gc00026b

www.rsc.org/greenchem

Introduction

Catalytic fast pyrolysis (CFP) is a technology for the production of monocyclic aromatics from solid biomass.¹ In a single step, up to 30% of the carbon contained within solid biomass is converted into aromatics including benzene, toluene, and xylenes (BTX). To perform CFP, biomass is fed into a fluidized bed of spray-dried zeolite catalyst where it thermally decomposes to form pyrolysis vapors. The pyrolysis vapors enter the zeolite's pores forming aromatics and olefins along with CO, CO₂, H₂O and char/coke. The solid char/coke accumulates on the catalyst surface and deactivates the catalyst, so it is necessary to send charred/coked catalyst to a furnace where the char/coke is combusted to provide process heat. The advantage of CFP is that pyrolysis and catalysis occur in a single reactor, which greatly reduces process cost. Furthermore, CFP produces commodity chemical products (aromatics and olefins) that already fit into existing infrastructure.^{1–9}

Previous research has focused on optimizing CFP reactor conditions,^{2,5,10–14} optimizing reactor configurations,^{2,7,15,16} screening and design of improved catalysts,^{3,17–23} investigating feedstocks,^{24–26} and determining the effects of inorganic contaminants.^{27–29} High temperatures (650 °C) are favorable for the production of olefins and CO, intermediate temperatures (450–600 °C) for aromatics, and low temperatures

(450 °C) for benzofuran and char/coke.¹¹ Carlson *et al.* obtained an aromatic yield of 14% C from pine sawdust in a bench-scale fluidized-bed reactor running at low biomass weight hourly space velocities (WHSV < 0.5 h⁻¹) and high temperature (600 °C).² Karanjkar *et al.* obtained an aromatic yield of 39.5% C from cellulose feed at similarly low space velocity (0.25 h⁻¹), but at lower temperature (500 °C), indicating that importance of cellulose over the other components of biomass.⁵ This increase is consistent with earlier results from Carlson *et al.* which indicated that choosing biomass feedstocks with high amounts of cellulose and hemicellulose will increase aromatic yield.²

Jae *et al.* carried out CFP of sawdust in a process development unit (PDU) consisting of a bubbling fluidized-bed reactor with continuous catalyst addition and removal, and was capable of maintaining constant product yield of aromatics (15.5% C) over an extended reaction period (6 h).⁴ Paasikallio *et al.* performed CFP of pine sawdust in a 20 kg h⁻¹ PDU riser reactor over a four-day run, and reported a pyrolysis-oil yield of 24% C.⁹

In contrast to fossil fuels, biomass feedstocks possess high contents of both moisture and oxygen.^{9,30,31} Drying and dehydration reactions produce large amounts of steam during CFP, much of which condenses as water in the liquid-phase products.³² Little is known about the effect of this steam on CFP chemistry. The presence of steam during un-catalyzed biomass pyrolysis is understood to change gas, char/coke, and liquid yields and promote the removal of oxygen from the liquid.³³ Williams *et al.* found that the presence of steam during zeolite-catalyzed upgrading of oxygenated biomass pyrolysis vapors led to the formation of large amounts of gaseous products with a yield in excess of 70% at 550 °C, proposing that

^aState Key Laboratory of Coal Combustion, Huazhong University of Science and Technology, Wuhan, 430074, China

^bDepartment of Chemical and Biological Engineering, University of Wisconsin-Madison, Madison, WI 53706, USA. E-mail: huber@enr.wisc.edu

^cDepartment of Chemical and Biological Engineering, University of Massachusetts-Amherst, Amherst, MA 01003, USA

water can act as H₂ donor.³⁴ Gilbert *et al.* studied the influence of water on the conversion of furan over ZSM-5 and found that water hydrolyzes furans to produce more propylene and CO₂.³⁵

In CFP, steam may also affect catalyst integrity. Iliopoulou *et al.* found that treatment of mesoporous Al-MCM-41 at 550 °C under a 20% steam atmosphere caused a significant reduction in acidity and porosity.³⁶ Ong *et al.* found that steam treatment of ZSM-5 for 5 h at 450 °C under a pure steam atmosphere caused irreversible dealumination through stable tetrahedrally-coordinated extra-framework aluminum neutralizing aluminum/oxygen tetrahedra in the lattice, thus reducing the number of Brønsted acid sites.³⁷ Corma *et al.* studied the steam catalytic cracking of naphtha over ZSM-5 at 650 °C with a steam vapor fraction between 0% and 35.7% and found their catalyst underwent intense dealumination, cracking rates decreased after steam exposure times of 600 s, and these effects are more apparent at higher temperatures.³⁸

In addition to steam causing irreversible dealumination, previous research has demonstrated reversible deactivation as it can compete with reactant species (specifically *n*-heptane) for adsorption on active sites, thus negatively affecting the catalyst's activity.³⁹ Corma *et al.* found that post-synthesis treatment with phosphorous, introduced to enhance the hydrothermal stability, slowed down catalyst deactivation for steam catalytic cracking.⁴⁰ Lee *et al.* found that the phosphorus-treated HZSM-5 (P/ZSM-5) exhibited lower acidity, higher hydrothermal stability and improved dimethyl ether (DME) selectivity in methanol conversion compared to the phosphorus-free HZSM-5.⁴¹

Zeolite catalysts used in fluidized beds are spray dried with a binder in order to obtain larger and more attrition-resistant particles with other desirable fluidization characteristics.⁴² The presence of binder can affect catalyst behavior through (1) changes in the proton-exchange efficiency, (2) blocking of the zeolite channels, and (3) channels in the binder trapping coke precursors which cause a significant decrease in the amount of coke deposited on the zeolite.^{43,44}

The objective of this paper is to elucidate the separate effects of (1) the long-term influences of steam's irreversible effects on the catalyst during CFP and how this affects product distribution, and (2) the interaction steam itself has with changing the product distribution through potentially acting as a homogeneous catalyst, a reactant species, or a heterogeneous catalyst site blocker.

Experimental

Materials

Industrial grade cellulose with an average particle size of 200 μm (Lattice® NT Microcrystalline Cellulose, FMC biopolymer, 99%) was used as the feedstock for this study. In all our calculations, the empirical formula C₆H₁₀O₅ was used for cellulose.

The catalyst used in these experiments was a commercial spray-dried 40% ZSM-5 catalyst (Intercat Inc.) with a particle-size average of 99 μm and standard deviation of 23 μm. Ninety

grams of catalyst were loaded into the reactor; a loading corresponding to roughly 15% of the reactor volume. Prior to reaction, the catalyst was calcined *in situ* at 600 °C in air flowing at 600 sccm.

Reactor setup

CFP of cellulose was performed in a fluidized-bed reactor system, as shown in Fig. 1. The fluidized bed reactor is a 316L stainless-steel 4.92 cm ID pipe with a freeboard height of 37 cm. Above the freeboard is a disengaging zone which expands to a 7.79 cm ID pipe. The catalyst bed is supported by a distributor plate made from two layers of 304 stainless-steel cloth (200 mesh) glued to a stainless-steel screen for support. The main reactor body and space beneath the distributor plate (henceforth referred to as the plenum) were sealed together using bolted flanges. The interior of the reactor and the plenum were spray-coated with a protective layer of abrasion-resistant ceramic to protect the reactor from corrosion.

The reactor and plenum were resistively heated using semi-circular ceramic heaters (WATLOW). The flanges joining the main reactor body and plenum were heated using a band heater. Heating-zone temperatures were controlled by thermocouples located between the reactor body and heaters.

A typical run was carried out for 30 min time on stream. The catalyst was fluidized using helium and/or steam at a rate of 600 sccm (henceforth referred to as the fluidizer gas). Heating of the plenum allowed for pre-heating of the fluidizer gas to the reaction temperature before reaching the catalyst. Steam was delivered to the reactor using a syringe pump and in-line steam kettle. A stainless steel auger equipped with a variable speed motor and rotary fitting fed cellulose into the side of the reactor. Cellulose was supplied to this auger *via* a sealed feed hopper (calibrated prior *via* balance and stopwatch). To maintain an inert environment and encourage the

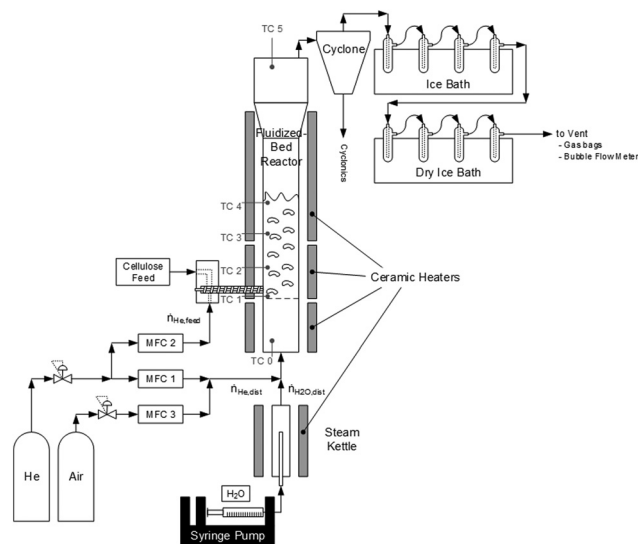


Fig. 1 Flow diagram of bubbling fluidized bed for catalytic fast pyrolysis (CFP).

rapid delivery of biomass to the reactor, the hopper and auger were swept with helium at a rate of 400 sccm (henceforth referred to as the feeding gas). Gas flows were selected to operate the reactor in the bubbling fluidized-bed regime. During the reaction, product gases exited the top of the reactor and were passed through a cyclone where entrained solids were removed as cyclonics. The solid-free vapors were then bubbled through four condensers each containing ~20 ml isopropanol maintained at 0 °C using an ice bath. Here, most organic species were captured through dissolution. The stream was then passed through four condensers maintained at -55 °C using a dry-ice/acetone bath to condense remaining organics. The non-condensable gases were then either vented, plumbed through a bubble flow meter, or sampled in Tedlar gas bags (Restek) for GC analysis. At the conclusion of cellulose feeding, the reactor was purged with 1000 sccm of helium for another 30 min to ensure a complete purge of all volatile organic products. The condensers were then removed and rinsed with isopropanol to collect all product liquids. The volume of isopropanol/product solution was recorded and analyzed *via* GC to quantify products.

After feeding and purge, the reactor temperature was increased to 600 °C, and the carrier gas was switched to air to combust char/coke and regenerate the catalyst. For a typical run, the catalyst was regenerated for approximately two hours to ensure complete combustion of any organic species remaining on the catalyst.

Product analysis

During catalyst regeneration, the combustion effluent containing CO, CO₂, and water was passed through a copper catalyst (13 wt% CuO on alumina, Sigma Aldrich) held at 250 °C to convert CO to CO₂. This stream was then passed through a Dryrite trap to remove water followed by a pre-weighed Ascarite trap to capture CO₂. Weights of the Ascarite trap before and after catalyst regeneration were used to determine the quantity of char/coke generated from the reaction.

The liquid product dissolved in isopropanol was analyzed for aromatics using a Shimadzu GC2010 system with an Agilent HP INNOWax column (60 m, 0.32 mm, 0.5 μm) and a flame ionization detector (FID). Column max temperature: 260 °C. Carrier gas: He. Injection mode: split ratio of 10. Temperature Procedure: Initial temperature 70 °C, hold time 10 min, then heated up to 95 °C at 2 °C min⁻¹, then heated up 240 °C at 15 °C and hold up for 10 min.

Non-condensable gases collected in gas bags at various times during the reaction were analyzed using refinery gas analyzer Shimadzu GC2014 system with (1) RestekRtx (RTX) - Alumina column and a flame-ionization (FID) detector to analyze methane and C₂-C₅ olefins and (2) RTX-MS-5A column and RTX-Q-plot column with a thermal-conductivity detector (TCD) to analyze CO and CO₂ respectively.

Catalyst characterization

A Perkin-Elmer-emission spectrometer plasma 400 was used to do elemental analysis of the catalyst. A 100 mg sample of cata-

lyst was completely dissolved in 2 ml of hydrofluoric acid (50%) and several drops of boric acid (7%) were added in order to protect against the formation of volatile SiF₄. The solution was heated at 80–90 °C for seven minutes to allow some of the hydrofluoric acid to evaporate before the solution was allowed to cool. About 2 ml of nitric acid (10%) and several ml of boric acid (7%) were added to the solution, then water was added to bring the solution volume to 50 ml.

The acidity of the samples was measured using Temperature Programmed Desorption (TPD) of isopropylamine (IPA-TPD) and ammonia (NH₃-TPD) using a Micromeritics® Autochem II 2920 with an inline Thermal Conductivity Detector (TCD). Before testing, the catalyst was heated up to 600 °C for 2 h in helium to remove adsorbed water or organic species. For IPA-TPD, once the 100 mg sample was saturated with IPA at 50 °C for 20 min, helium was flushed at 50 sccm for 2 h in the temperature range of 50–700 °C at a heating rate of 10 °C min⁻¹. For NH₃-TPD, once the 100 mg sample was saturated with NH₃ at 100 °C for 30 min, helium was flushed at 12 sccm for 2 h in the temperature range of 150–700 °C at a heating rate of 5 °C min⁻¹. The number of Brønsted acid sites was calculated based on the TCD signal for NH₃ and propylene, the products of IPA decomposition. The total number of acid sites was calculated based on the TCD signal for NH₃. The number of Lewis acid sites was taken as the difference between the total number of acid sites and the number of Brønsted acid sites.

The zeolite crystallinity was determined by a Bruker D8 Discover diffractometer using CuKα radiation (*l* = 1.542 Å). The scattering angle 2θ was varied from 5° to 60°. The crystal size was calculated using the Scherrer equation.

The BET surface area and pore volume of the samples were calculated by N₂ adsorption/desorption isotherms obtained at -196 °C using a Micromeritics, ASAP2020 adsorption analyzer. Prior to N₂ adsorption, the samples were degassed at 300 °C overnight under vacuum.

The particle size distribution and surface morphology of catalyst was measured with a scanning electron microscope (SEM, LEO 1550 VP).

Definitions

The weight hourly space velocity (WHSV) of cellulose was calculated by dividing the cellulose mass flow rate by the mass of catalyst present inside the fluidized bed reactor as shown in eqn (1). Selectivity towards a particular aromatic compound is defined in eqn (2) by dividing the number of moles of carbon in that aromatic product by the number of moles of carbon in all the aromatic products. eqn (3) defines selectivity towards olefin compounds in a similar way.

$$\text{WHSV}(\text{h}^{-1}) = \frac{\text{cellulose flow rate} (\text{g h}^{-1})}{\text{weight of catalyst} (\text{g})} \quad (1)$$

$$\text{Aromatic selectivity} = \frac{\text{moles of carbon in aromatic product}}{\text{moles of carbon in all aromatic products}} \times 100\% \quad (2)$$

$$\text{Olefin selectivity} = \frac{\text{moles of carbon in olefin product}}{\text{moles of carbon in all olefin products}} \times 100\% \quad (3)$$

Method for estimation of an average bubble size and expanded bed height

The assemblage model, as described by Karanjkar *et al.*⁵ was used to determine the influence of steam on the hydrodynamic properties. Hydrodynamic properties such as bubble size, bubble velocity, residence time, and density of fluidization were calculated from inputs such as bed temperature, particle size, bed weight, output fluidizer flowrate, and input fluidizer composition. The model was expanded to include changes to gas density and viscosity based on its steam/helium makeup.

Results and discussion

Effect of steam vapor fraction on product yields and selectivity

To test the effect of steam's presence on CFP of cellulose, some fraction of the input carrier helium gas was replaced with an equivalent molar flowrate of steam. The fraction of steam was varied over a range of 0% to 60%. This upper bound of 60% represents a fluidization gas completely made up of steam (600 sccm) and a feed gas consisting of helium (400 sccm). The hydrodynamic parameters are listed in Table 1. Average bubble size, rise velocity and residence times for each phase were affected more-so by outlet gas flow rate than input composition. Regardless, all of these hydrodynamic properties were predicted to remain relatively stable throughout the range of vapor fraction tested.

Fig. 2 shows the product carbon yields at different steam vapor fractions in the range of 0–41%. A fresh catalyst was loaded into the reactor prior to each reaction test. The main products include aromatics, olefins, CH₄, CO, CO₂, char/coke, and some light oxygenates. The aromatics consisted of benzene, toluene, ethyl-benzene, xylenes, styrene, indene, and naphthalene. The identifiable oxygenates consisted of benzo-

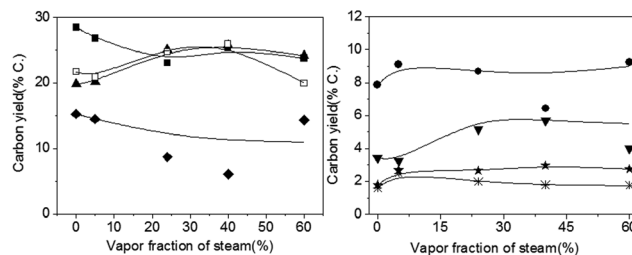


Fig. 2 Carbon yield as function of input vapor fraction of steam for catalytic fast pyrolysis of cellulose with fresh ZSM-5 catalyst. (Reaction conditions: Cellulose feed, WHSV: 0.4 h⁻¹, Temperature: 500 °C, time on stream: 30 min, 90 g catalyst.) ■: Aromatics, ▲: CO, ◆: Char/coke, ●: Olefins, ▼: CO₂, ★: Methane, *: Identifiable Oxygenates, □: Unidentified carbon.

furan, phenol, acetaldehyde, acetic acid, hydroxyacetone, and 5-hydroxymethyl furfural.

The aromatic yield decreased linearly from 28% C to 22% C as input vapor fraction of steam increased from 0% to 24%, but remained close to 22% C with further increases to steam vapor fraction. Carbon monoxide showed a trend contrary to aromatics, increasing with steam vapor fraction (perhaps as H₂O reacted with char/coke precursors) up to 24% steam. The char/coke yield decreased from 15% C to 5% C as the steam fraction increased from 0% to 40% and then it increased with further steam vapor fraction. Olefins, methane, and identifiable oxygenate yields showed no obvious change with steam vapor fraction. The yield of unidentified carbon not detected in any of the product phases (calculated as the balance carbon of the cellulose feed, presumed to be larger oxygenated compounds) increased with increasing steam vapor fractions of steam and reaching the maximum value at 27% C, and then decreasing.

The aromatics selectivity did not change with input vapor fraction of steam, as shown in Fig. 3. Benzene and toluene were the two main liquid products at these reaction conditions, each with a selectivity of about 35% C. However, the olefin selectivity did change with steam vapor fraction, as shown in Fig. 4. Increasing the steam vapor fraction increased the ethylene selectivity and decreased the propylene selectivity.

Table 1 Estimated average bubble size, bubble residence time, and expanded bed height as estimated from the Assemblage Model.⁵ Reaction conditions: Cellulose feed, WHSV: 0.4 h⁻¹ Temperature: 500 °C, time on stream: 30 min, 90 g catalyst. Fluidizer gas: He/Steam mix @ 600 sccm, Feed Gas: He @ 400 sccm

Parameter	Definition	Result				
Input steam fraction (%)	Flow rate of steam/(Fluidizer gas + Feed gas)	0.00%	5.00%	24.00%	40.00%	60.00%
Outlet gas flowrate (sccm)	Measured by volume flow meter	1608.57	1666.67	1715.42	1437.71	1479.46
$d_{b,ave}$ (cm)	Bubble diameter, averaged over the height of the bed	0.83	0.85	0.87	0.80	0.81
$u_{b,ave}$ (cm s ⁻¹)	Bubble rise velocity, averaged over the height of the bed	33.02	33.46	33.83	32.04	32.30
δ (%)	Fraction of the bed occupied by the bubble phase	11.61	11.98	12.28	10.79	11.01
L_f (cm)	Height of fluidized bed	8.55	8.59	8.62	8.47	8.49
Expansion (%)	% height increase from packed to fluidized bed	41.41	42.01	42.50	40.12	40.47
τ_f (s)	Average gas residence time in the fluidized bed	1.20	1.16	1.14	1.32	1.29
τ_e (s)	Gas residence time in the emulsion phase	19.18	22.35	26.18	26.65	25.73
τ_b (s)	Gas residence time in the bubble phase	0.26	0.26	0.26	0.27	0.27

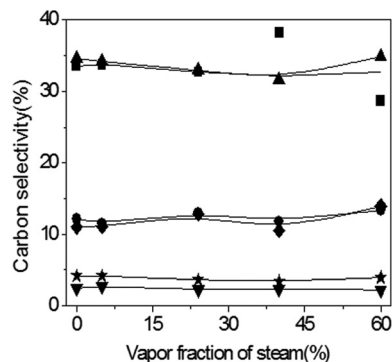


Fig. 3 Aromatic carbon selectivity as function of input vapor fraction of steam for catalytic fast pyrolysis of cellulose with ZSM-5 catalyst. (Reaction conditions: Cellulose feed, WHSV: 0.4 h^{-1} , Input steam fraction: 60%, Temperature: $500 \text{ }^\circ\text{C}$, time on stream: 30 min, 90 g catalyst.) ■: Benzene, ▲: Toluene, ◆: Xylenes + Ethylbenzene, ●: Naphthalenes, ▼: Styrene, ★: Indene.

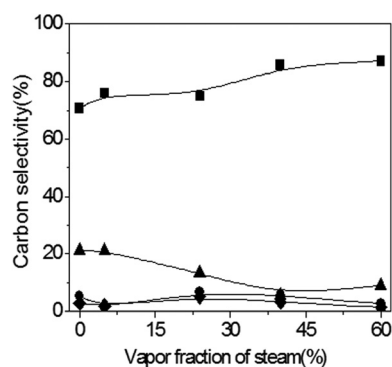


Fig. 4 Olefin carbon selectivity as function of input vapor fraction of steam for catalytic fast pyrolysis of cellulose with ZSM-5 catalyst. (Reaction conditions: Cellulose feed, WHSV: 0.4 h^{-1} , Input steam fraction: 60%, Temperature: $500 \text{ }^\circ\text{C}$, time on stream: 30 min, 90 g catalyst.) ■: Ethylene, ▲: Propylene, ◆: Butenes, ●: Pentenes.

The amount of butenes and pentenes was very low and no clear change was shown with respect to steam vapor fraction.

Effects of alternating no-steam and steam

The data in the previous section were collected with fresh catalyst for each run. These data offered little insight as to whether these trends were driven due to steam causing irreversible changes to the catalyst, or steam itself interfering with the reactions of pyrolysis and/or catalysis. To elucidate this matter, a series of cellulose CFP reactions were performed over a single 90 g batch of catalyst wherein the fluidizer gas was alternated as helium and steam (Temp. = $500 \text{ }^\circ\text{C}$, WHSV = 0.4 h^{-1} , time-on-stream = 30 min, fluidizer flow = 600 sccm.) At the conclusion of these “no-steam/steam runs”, the catalyst had been exposed to steam for a total of 330 min, though the catalyst had been run through cellulose CFP for a time roughly twice that. A small amount of catalyst ($\sim 1.0 \text{ g}$) was extracted after each steam run for analysis.

Influence of steam on catalyst

Brønsted : Lewis ratio via TPD. Fig. 5 shows the catalyst acidity as a function of steam exposure time during cellulose CFP. The Brønsted acidity undergoes a 25% decrease during the first 30 min of steam exposure followed by a gradual decrease. The Lewis acidity increased with steam exposure, suggesting that Brønsted sites converted to Lewis sites as the catalyst underwent dealumination as described by Ong *et al.*³⁷ The total acidity of the catalyst decreased from $114 \mu\text{mol g}^{-1}$ to $42 \mu\text{mol g}^{-1}$. This analysis shows that the most significant acidity changes occur during the initial 30 min of exposure to steam.

Si : Al ratio via ICP. As shown in Fig. 6, ICP analysis showed that the Al and Si content within the catalyst (consisting of both zeolite and binder) did not change after steam exposure. Other researchers observed loss of framework aluminum in the presence of steam, though at higher temperatures. Corma *et al.* found that a 35% steam atmosphere can remove some

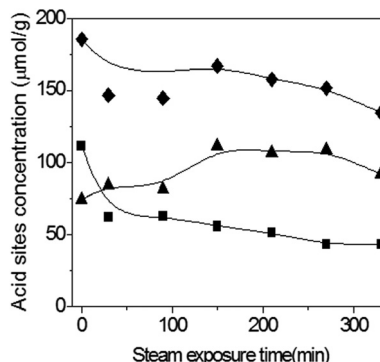


Fig. 5 Catalyst acid-site concentration as a function of steam exposure time. (Reaction conditions: Cellulose feed, WHSV: 0.4 h^{-1} , Input steam fraction: alternating between 0% and 60%, Temperature: $500 \text{ }^\circ\text{C}$, time on stream: 30 min, 90 g catalyst.) ■: Brønsted sites, ▲: Lewis sites, ◆: Total acid sites.

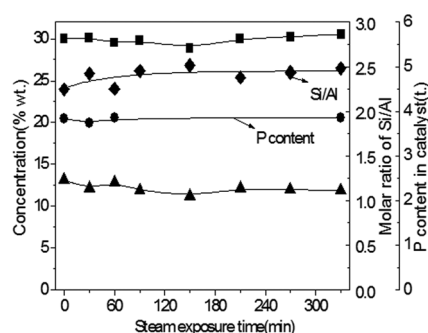


Fig. 6 ZSM-5 Si and Al concentrations as a function of steam exposure time. (Reaction conditions: Cellulose feed, WHSV: 0.4 h^{-1} , Input steam fraction: alternating between 0% and 60%, Temperature: $500 \text{ }^\circ\text{C}$, time on stream: 30 min, 90 g catalyst.) ■: Si concentration, ▲: Al concentration, ◆: Si : Al molar Ratio, ●: P concentration.

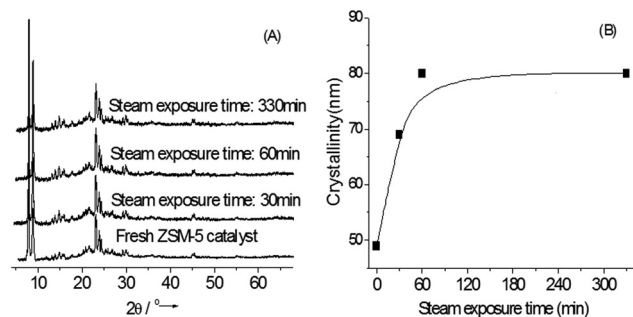


Fig. 7 XRD pattern of steamed ZSM-5 catalyst. (Reaction conditions: Cellulose feed, WHSV: 0.4 h^{-1} , Input steam fraction: alternating between 0% and 60%, Temperature: $500 \text{ }^\circ\text{C}$, time on stream: 30 min, 90 g catalyst.) A: XRD pattern; B: Crystallinity of ZSM-5 catalyst.

ZSM-5 framework Al during catalytic cracking of naphtha for production of propene and ethane at $500\text{--}700 \text{ }^\circ\text{C}$ when vapor fractions of steam exceed 17.8%.³⁸ Iliopoulou *et al.* also found that steam presence decreases the acidity and Al content of MCM-41 at $550 \text{ }^\circ\text{C}$ and $750 \text{ }^\circ\text{C}$ for vapor fractions of steam of 20%.³⁶

The phosphorus content was also measured *via* ICP and found to be stable with steaming, remaining at a value of $\sim 3.85 \text{ wt}\%$ as shown in Fig. 6. Both binder and phosphorus have been reported to inhibit the volatilization of framework aluminum *via* steaming.^{41,45}

Crystallinity *via* XRD. The powder XRD patterns of the steamed ZSM-5 samples are shown in Fig. 7. The intensity and peak positions of all of the zeolite samples are in good agreement with previously reported spectra, including typical diffraction peaks at $2\theta = 7.88^\circ$ (011), 8.76° (020), 23.0° (501), 23.84° (033) and 24.3° (133).^{46,47} No change in the XRD peak positions or new peaks appeared after steam exposure. However, the zeolite crystal size increased from $\sim 50 \text{ nm}$ to $\sim 80 \text{ nm}$ after a steam exposure time of 60 min and remained stable with further steaming as shown in Fig. 7B. This decrease in crystallite size may cause further decreases in catalyst activity by decreasing diffusion limitations.^{48–50}

Porosity *via* nitrogen adsorption. The BET surface area and pore volume distribution based on liquid N_2 isothermal adsorption at $-196 \text{ }^\circ\text{C}$ are shown in Table 2 and Fig. 8, as

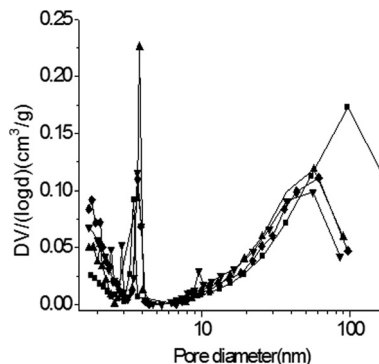


Fig. 8 Mesopore size distributions determined from BJH adsorption. (Reaction conditions: Cellulose feed, WHSV: 0.4 h^{-1} , Input steam fraction: alternating between 0% and 60%, Temperature: $500 \text{ }^\circ\text{C}$, time on stream: 30 min, 90 g catalyst.) ■: fresh catalyst, ▲: 30 min of steaming, ▼: 60 min of steaming, ◆: 330 min of steaming.

calculated from methods described by Sing *et al.*⁵¹ The BET surface area, the micropore ($<2 \text{ nm}$) area, and the mesopore ($3\text{--}4 \text{ nm}$) volume increased during the first 30 min of steaming. As micro- and mesopores are necessary for the formation of aromatics, this increased pore population most likely increases the formation of aromatic products.¹⁹ In contrast, the volume of macropores ($>50 \text{ nm}$) decreased with steaming in the first 30 min. Since these large pores are located between zeolite crystals and within the binder, this suggests that macropores collapsed with steam exposure, a finding which is consistent with the increase in zeolite crystallite size as shown from the XRD measurements. With fewer macropores, micropores are more susceptible to blockage by char/coke, thus inhibiting the formation of the hydrocarbon pool, and lowering the catalyst activity.^{52,53} The micropore area and micropore volume both decreased below their initial values at 330 min steam exposure time. The population of large macropores ($>50 \text{ nm}$) did not change substantially after its initial change within the first 30 min, suggesting that at this time the macropores had finished collapsing and the zeolite crystals began the process of fusing. The SEM images shown in Fig. 9 qualitatively further confirmed this result.

Particle size distribution and physical integrity *via* SEM. The particle size distribution was determined *via* SEM

Table 2 BET surface area and pore volume parameters of steamed catalyst. (Reaction conditions: Cellulose feed, WHSV: 0.4 h^{-1} , Input steam fraction: alternating between 0% and 60%, Temperature: $500 \text{ }^\circ\text{C}$, time on stream: 30 min, 90 g catalyst.)

Sample	BET surface area ($\text{m}^2 \text{ g}^{-1}$)	External surface area ^a ($\text{m}^2 \text{ g}^{-1}$)	Micropore area ^a ($\text{m}^2 \text{ g}^{-1}$)	Micropore volume (cc g^{-1})	Average pore size (nm)
Fresh catalyst	108.86	36.93	130.19	0.040	7.06
30 min	156.10	38.44	187.89	0.0598	4.49
60 min	145.67	50.89	219.11	0.0486	3.73
330 min	109.48	49.81	112.61	0.0314	5.13

^a External surface area, micropore area, and pore volume derived based on *t*-plot method, Average pore size is calculated with $4 V A^{-1}$ by BET. Determined from the N_2 isothermal uptake at $P/P_0: 0.10\text{--}0.90$ at $-196 \text{ }^\circ\text{C}$.

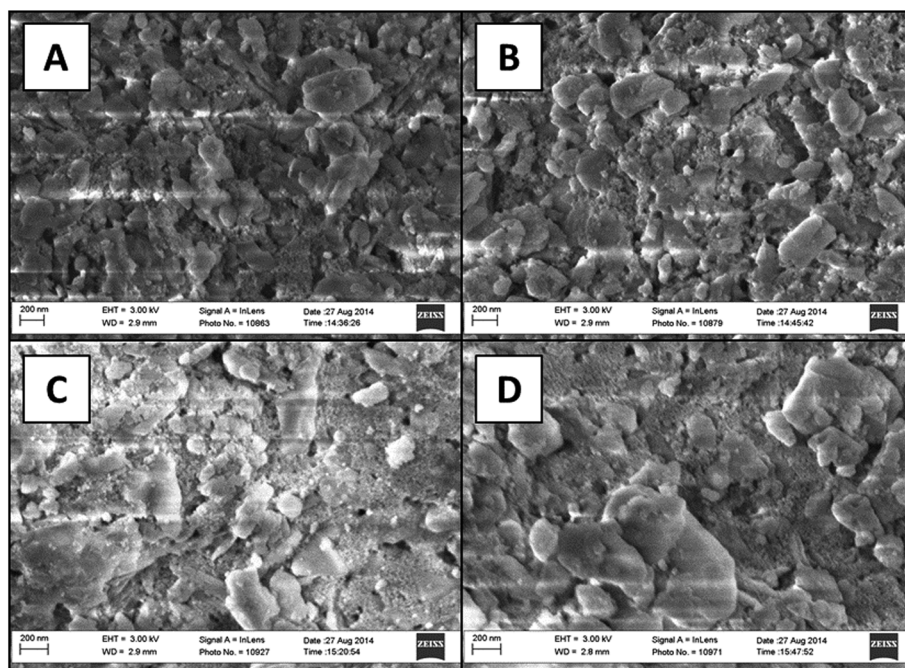


Fig. 9 Surface morphology of steamed catalyst based on SEM. (Reaction conditions: Cellulose feed, WHSV: 0.4 h^{-1} , Input steam fraction: alternating between 0% and 60%, Temperature: $500 \text{ }^\circ\text{C}$, time on stream: 30 min, 90 g catalyst.) A: fresh catalyst, B: 30 min of steaming, C: 60 min of steaming, D: 330 min of steaming.

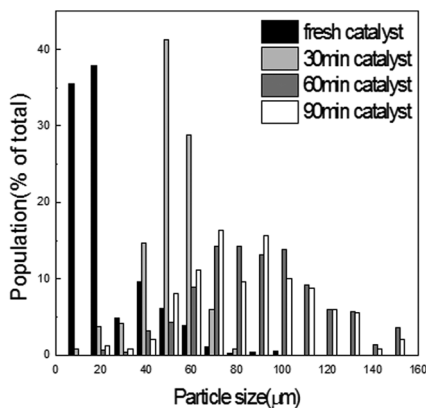


Fig. 10 Particle size distribution of steamed catalyst based on SEM. (Reaction conditions: Cellulose feed, WHSV: 0.4 h^{-1} , Input steam fraction: alternating between 0% and 60%, Temperature: $500 \text{ }^\circ\text{C}$, time on stream: 30 min, 90 g catalyst.)

as shown in Fig. 10 and 11. Fresh catalyst particles are almost exclusively spherical, but with a large fraction of fines ($<20 \mu\text{m}$). In the first 30 min of steaming, the largest difference is the loss of these fines, though the peak population size above $20 \mu\text{m}$ does increase slightly from $40 \mu\text{m}$ to $50 \mu\text{m}$, suggesting that the particles are already beginning to agglomerate. With further steam exposure (60 min), the particles agglomerated further and shifted the peak population size to $90 \mu\text{m}$. More irregularly-shaped particles appear as smaller particles become agglomerated with larger particles

as shown in Fig. 11. Above a steam exposure time of 60 min, the particles appear to have finished agglomerating, as the peak population size remains at $90 \mu\text{m}$. Past 60 min however, more catalyst fragments appear, suggesting that catalyst attrition becomes important at longer durations of use, though this will be true regardless of whether there is steam present in the reactor.

Influence of steam on product yields. Fig. 12 shows the progress of product yields for the alternating no-steam/steam runs as a function of steam-exposure time. The data have been separated into runs performed without steam co-feeding (Fig. 12A and C) and with steam co-feeding (Fig. 12B and D). Clearly, steaming changes the product yield. For the CFP runs without steam co-feeding, the yield of aromatics decreased gradually from 29% C to 18% C over the course of steaming. The char/coke yield decreased from 15% C to 7.8% C over the course of steaming, while the olefin and methane yields showed a gradual increase. The CO and CO₂ both went through a maximum yield at 60 min and 30 min of steaming respectively, gradually decreasing thereafter. The identified oxygenates increased slightly from 1.5% C to 3% C in the first 60 min but remained stable thereafter. The results indicate that the product yields are greatly affected by the structural changes to the catalyst induced by steam exposure, as most changes to the catalyst properties do change before 90 min of steam exposure as shown in Fig. 5 through 11. The pore-size distribution doesn't change after 30 min of steam exposure, crystal growth stops occurring after 60 min steam exposure, and the particle size distribution doesn't change after 60 min steam exposure.

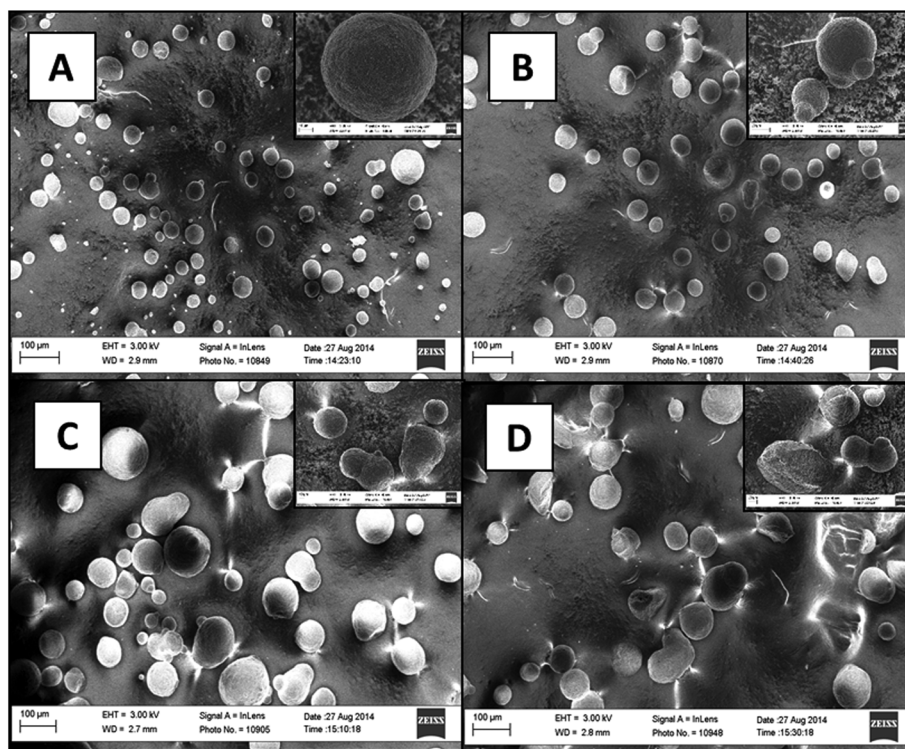


Fig. 11 SEM images of typical catalyst particles at various stages of steaming. Inset photos show examples of various stages of particle agglomeration. (Reaction conditions: Cellulose feed, WHSV: 0.4 h^{-1} , Input steam fraction: alternating between 0% and 60%, Temperature: $500 \text{ }^\circ\text{C}$, time on stream: 30 min, 90 g catalyst.) A: fresh catalyst, B: 30 min of steaming, C: 60 min of steaming, D: 330 min of steaming.

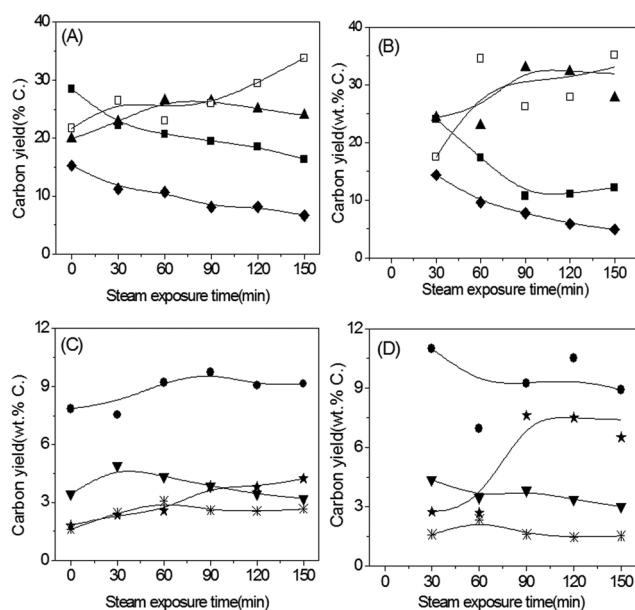


Fig. 12 Carbon yield as function of catalyst steam exposure time for catalytic fast pyrolysis of cellulose with ZSM-5 catalyst. (Reaction conditions: Cellulose feed, WHSV: 0.4 h^{-1} , Input steam fraction: alternating between 0% and 60%, Temperature: $500 \text{ }^\circ\text{C}$, time on stream: 30 min, 90 g catalyst.) A,C: Without steam co-feeding; B,D: With steam co-feeding. ■: Aromatics, ▲: CO, ◆: Char/coke, □: Unidentified carbon, ●: Olefins, ▼: CO_2 , ★: Methane, *: Identifiable Oxygenates.

Past steam exposure times of 60 min, the yields of aromatics, coke/char, CO, and CO_2 seem to correlate with decreases in Brønsted acidity. The unidentified balance carbon increased with steam exposure, suggesting that heavier unidentifiable oxygenated species were produced in greater amounts as the catalyst underwent these changes.

For CFP runs with steam co-feeding, the changes in the product yield can be divided into two ranges: before and after the first 90 min. With steam co-feeding, the carbon yield of aromatics decreased from 24% C to 10% C in the first 90 min, but remained constant after. CO and methane showed the opposite tendency and their yields became enhanced particularly in the first 90 min, and remained somewhat constant with further steaming. With steam co-feeding, the char/coke yield decreased gradually from 15% C to 5% C over the entire 150 min of steam exposure. The CO_2 yield slightly decreased from 4% to 3%. The olefin yield for steam co-feeding did decrease over the span of steaming, though these results are noisy in the range of <90 min, so it cannot be said whether this change was abrupt (as with aromatics, CO and methane), or gradual (as with char/coke and CO_2). The identifiable oxygenate species yield was stable at about 1.5% C. As was the case without steam co-feeding, unidentified balance carbon increased with steam exposure, again suggesting that heavier unidentifiable oxygenated species were produced in greater amounts as the catalyst underwent changes.

Influence of steam on aromatic and olefin selectivities. The aromatic selectivity changed over the course of steam-exposure time as shown in Fig. 13. For runs without steam co-feeding (Fig. 13A), the aromatic selectivities did not change. For runs with steam co-feeding (Fig. 13B), the first 90 min of steaming caused the benzene selectivity to increase and the toluene selectivity to decrease. The carbon selectivity of xylenes decreased while that of styrene increased in that same period. The naphthalenes and indene selectivities did not change. After 90 min of steam exposure, all the selectivities were fairly constant. These results suggest that changes to the catalyst (such as decreases in the amount of Brønsted acidity, shrinking of mesopore area, and increases in zeolite crystallinity) did not show great influence on aromatics selectivity, but the presence of steam did enhance the formation of toluene over benzene in the first 30 min.

The ethylene selectivity increased and the propylene selectivity decreased with steam exposure time for runs both with and without steam co-feeding as shown in Fig. 14.

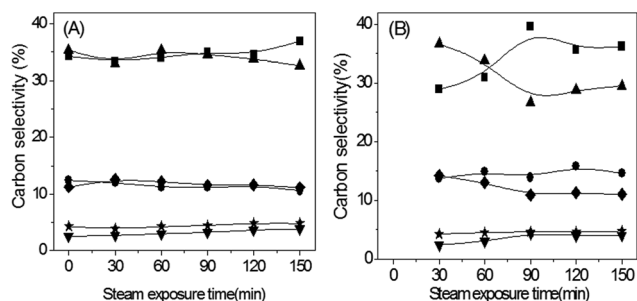


Fig. 13 Aromatic carbon selectivity as function of steam co-feeding time for catalytic fast pyrolysis of cellulose with ZSM-5 catalyst. (Reaction conditions: Cellulose feed, WHSV: 0.4 h^{-1} , Input steam fraction: alternating between 0% and 60%, Temperature: $500 \text{ }^\circ\text{C}$, time on stream: 30 min, 90 g catalyst.) A: Without steam co-feeding; B: With steam co-feeding. ■: Benzene, ▲: Toluene, ◆: Xylenes + Ethylbenzene, ●: Naphthalenes, ▼: Styrene, ★: Indene.

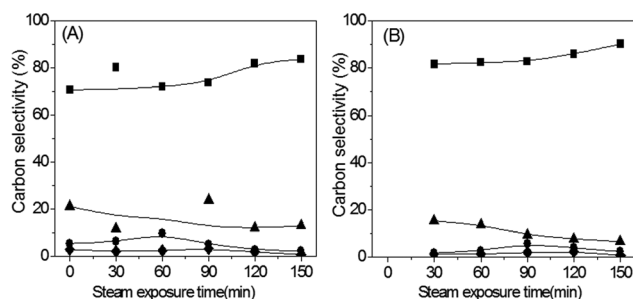


Fig. 14 Olefin carbon selectivity as function of steam co-feeding time for catalytic fast pyrolysis of cellulose with ZSM-5 catalyst. (Reaction conditions: Cellulose feed, WHSV: 0.4 h^{-1} , Input steam fraction: alternating between 0% and 60%, Temperature: $500 \text{ }^\circ\text{C}$, time on stream: 30 min, 90 g catalyst.) A: Without steam co-feeding; B: With steam co-feeding. ■: Ethylene, ▲: Propylene, ◆: Butenes, ●: Pentenes.

The shift in both data sets is similar, even though steam co-feeding consistently produces more ethylene than without steam co-feeding. In both cases, the yields of butenes and pentenes is quite low ($<1\% \text{ C}$), and steam co-feeding had no observable effect during the process of cellulose CFP.

Influence of steam on homogeneous and heterogeneous reactions

Student's *t*-test was performed to distinguish between (1) the long-term influences of steam's irreversible effects on the catalyst during CFP and how this affects product distribution, and (2) the interaction steam itself has with changing the product distribution through potentially acting as a homogeneous catalyst, a reactant species, or a heterogeneous catalyst site blocker. The results are shown in Table 3. Three runs were taken from each no-steam/steam data set. In each case, the data selected had a steam exposure time greater than 90 min because before this point, product yields changed too rapidly for an average to have any meaning. Although product yields do change after 90 min, for the runs selected, an average is representative. The average (\bar{x}) and standard deviation (*s*) are shown for each group and compound in each data set. Also shown is the *t*-statistic (*t*) and whether this value is statistically significant to within 95% confidence (and in which direction). Within the confines of 95% confidence, steam co-feeding was found to decrease the yields of aromatics, char/coke, and identifiable oxygenates, and increase the yields of methane and CO. No measurable change in the yield of CO_2 was observed.

Steam co-feeding decreased the yield of all aromatics species except naphthalene, though any changes to olefin yield were not statistically significant. For oxygenates, steam co-feeding decreased the yield of acetaldehyde, furan and hydroxyacetone, though no measurable influence was observed for other oxygen-containing species detected.

Worth noting is the near statistical significance in the yield changes in ethylene and propylene. While the effects at this level of confidence are not measurable within this sample size, these results do suggest that there may be an effect of steam co-feeding that causes an increase in the yield of ethylene and a decrease in the yield of propylene. These results run contrary to the work of Gilbert *et al.* who showed for furan CFP, more propylene is formed with steam co-feeding.³⁵ While this disparity might be attributable to differences in operating temperature and/or vapor residence time, a stronger implication is that cellulose does not form a furan-related intermediate during CFP.

In comparison with steam co-feeding, the carbon yield of aromatics, char/coke and oxygenates showed higher yields, while that of CO and methane is lower for the run without steam co-feeding for each catalyst with same steam exposure time. We speculate that steam is competing with pyrolytic vapors for adsorption on active sites and therefore reversibly blocking the catalytic sites.³⁸ Also the presence of steam might dilute the concentration of aromatics intermediates/pyrolytic

Table 3 The influence of steam on cellulose CFP based on Student's *t*-test (Reaction conditions: Cellulose feed, WHSV: 0.4 h⁻¹, Input steam fraction: alternating between 0% and 60%, Temperature: 500 °C, time on stream: 30 min, 90 g catalyst.) \bar{x} = sample mean, *s* = sample standard derivation, *t* = *t*-statistic, 1- α = confidence level, *t*_{crit} = threshold of statistical significance according to chosen α . "↑" indicates a statistically significant increase, "↓" indicates a statistically significant decrease, and "—" indicates no statistically significant change

	No steam, <i>n</i> = 3		Steam, <i>n</i> = 3		<i>t</i>	α = 5% <i>t</i> _{crit} = ±2.78
	\bar{x}	<i>s</i>	\bar{x}	<i>s</i>		
All	Yield (%C)		Yield (%C)			
Aromatics	17.46%	1.65%	11.16%	0.58%	-6.24	↓
Olefins	9.31%	0.36%	10.16%	1.09%	1.28	—
Id. oxygenates	3.26%	0.09%	2.06%	0.07%	-18.22	↓
CO	25.16%	1.25%	31.89%	3.94%	2.82	↑
CO ₂	3.49%	0.33%	3.54%	0.65%	0.12	—
Char/coke	7.62%	0.84%	5.51%	0.51%	-3.7	↓
Methane	3.95%	0.24%	7.45%	0.92%	6.39	↑
TOTAL	70.24%	3.92%	71.77%	6.76%	0.34	—
Aromatics	Yield (%C)		Yield (%C)			
Benzene	6.19%	0.41%	3.94%	0.23%	-8.19	↓
Toluene	5.89%	0.72%	3.19%	0.20%	-6.28	↓
Xylenes	1.58%	0.23%	0.89%	0.05%	-5.1	↓
Naphthalene	1.94%	0.25%	1.82%	0.25%	-0.59	—
Ethyl-benzene	0.42%	0.02%	0.36%	0.03%	-3.96	↓
Styrene	0.62%	0.02%	0.44%	0.03%	-8.72	↓
Indene	0.82%	0.06%	0.52%	0.04%	-7.31	↓
Total aromatics	17.46%	1.65%	11.16%	0.58%	-6.24	↓
Olefins	Yield (%C)		Yield (%C)			
C ₂	7.33%	0.49%	9.06%	1.02%	2.64	—
C ₃	1.49%	0.61%	0.73%	0.12%	-2.12	—
C ₄	0.18%	0.11%	0.14%	0.11%	-0.47	—
C ₅	0.31%	0.14%	0.23%	0.18%	-0.58	—
Total olefins	9.31%	0.22%	10.16%	0.38%	1.28	—
Id. oxygenates	Yield (%C)		Yield (%C)			
Benzofuran	0.22%	0.01%	0.20%	0.00%	-2.24	—
Phenol	0.45%	0.05%	0.41%	0.02%	-1.49	—
Hydroxyacetone	0.11%	0.01%	0.06%	0.02%	-4	↓
HMF	0.60%	0.04%	0.63%	0.10%	0.4	—
Acetaldehyde	0.85%	0.04%	0.43%	0.08%	-8.47	↓
Furan	0.96%	0.09%	0.31%	0.08%	-9.6	↓
2-MF	0.05%	0.09%	0.02%	0.04%	-0.53	—
Acetic acid	0.01%	0.00%	0.01%	0.01%	-2.35	—
Total Id. oxygenates	3.26%	0.09%	2.06%	0.07%	-18.22	↓

vapors, thus lowering aromatics conversion and decreasing aromatics and char/coke yields.³⁹ However, the presence of steam might enhance steam-shifting and methanation of pyrolytic vapors and char/coke to form more CO and CH₄, an effect that will be more apparent after the irreversible effects of steam on the catalyst are complete.³⁴

Conclusion

Steam's effect on catalytic fast pyrolysis of cellulose was studied at 500 °C using a ZSM-5 catalyst in a bubbling fluidized bed reactor. Steam affects CFP through (1) irreversible changes to the catalyst structure and (2) direct interference through changing chemistries of pyrolysis and/or catalysis.

Steam caused dealumination and a conversion of Brønsted acidity to Lewis acidity. In the first 60 min of steam exposure, the catalyst was also found to change in pore structure as more fine mesopores formed at the cost of larger mesopores in the binder. Exposure of the catalyst to steam increased the zeolite crystal size. Furthermore, the catalyst particles agglomerated to form larger particles with steam co-feeding.

These irreversible catalyst changes were observed to effect product yields, both with and without steam co-feeding. In both cases, steamed catalyst had a lower aromatics and char/coke yield and a higher methane and unidentified products yield.

Reversible effects of steam co-feeding were also observed. Steam co-feeding lowers yields of aromatics, char/coke, and

identifiable oxygenate species, increases yields of CO and methane, and does not change the overall yields of CO₂ and olefins. The data suggest that steam co-feeding favors the production of ethylene over propylene, but more data are required to confirm this finding.

Acknowledgements

This work was primarily funded by the National Science Foundation Office of Emerging Frontiers in Research and Innovation (EFRI) grant number 0937895. The first author also received support from Guangzhou Science and Technology Program key projects (National 973 project: no. 2013CB228102) and National Natural Science Foundation of China (no. 51376076). We would like to thank Dr Hyung Ju Kim for the SEM measurement and discussion about these results. Professor G.W. Huber has an ownership interest in Anellotech, which has licensed the technology reported in this publication.

Notes and references

- 1 T. Dickerson and J. Soria, *Energies*, 2013, **6**, 514–538.
- 2 T. R. Carlson, Y. T. Cheng, J. Jae and G. W. Huber, *Energy Environ. Sci.*, 2011, **4**, 145–161.
- 3 Y. T. Cheng, J. Jae, J. Shi, W. Fan and G. W. Huber, *Angew. Chem., Int. Ed.*, 2012, **51**, 1387–1390.
- 4 J. Jae, R. Coolman, T. J. Mountziaris and G. W. Huber, *Chem. Eng. Sci.*, 2014, **108**, 33–46.
- 5 P. U. Karanjkar, R. J. Coolman, G. W. Huber, M. T. Blatnik, S. Almalkie, S. M. de Bruyn Kops, T. J. Mountziaris and W. C. Conner, *AIChE J.*, 2014, **60**, 1320–1335.
- 6 G. Yildiz, M. Pronk, M. Djokic, K. M. van Geem, F. Ronsse, R. van Duren and W. Prins, *J. Anal. Appl. Pyrolysis*, 2013, **103**, 343–351.
- 7 H. Y. Zhang, R. Xiao, B. S. Jin, D. K. Shen, R. Chen and G. M. Xiao, *Bioresour. Technol.*, 2013, **137**, 82–87.
- 8 X. Wu, J. Markham, X. S. Sun and D. Wang, *T Asabe*, 2012, **55**, 1879–1885.
- 9 V. Paasikallio, C. Lindfors, E. Kuoppala, Y. Solantausta, A. Oasmaa, J. Lehto and J. Lehtonen, *Green Chem.*, 2014, **16**, 3549–3559.
- 10 H. Y. Zhang, Y. T. Cheng, T. P. Vispute, R. Xiao and G. W. Huber, *Energy Environ. Sci.*, 2011, **4**, 2297–2307.
- 11 Y. T. Cheng and G. W. Huber, *ACS Catal.*, 2011, **1**, 611–628.
- 12 P. A. Horne, N. Nugranad and P. T. Williams, *J. Anal. Appl. Pyrolysis*, 1995, **34**, 87–108.
- 13 N. Y. Chen, T. F. Degnan and L. R. Koenig, *Chem. Technol.*, 1986, **16**, 506–511.
- 14 M. Olazar, R. Aguado, M. J. San Jose and J. Bilbao, *J. Chem. Technol. Biotechnol.*, 2001, **76**, 469–476.
- 15 C. A. Mullen, A. A. Boateng, D. J. Mihalcik and N. M. Goldberg, *Energy Fuels*, 2011, **25**, 5444–5451.
- 16 J. Adam, E. Antonakou, A. Lappas, M. Stocker, M. H. Nilsen, A. Bouzga, J. E. Hustad and G. Oye, *Microporous Mesoporous Mater.*, 2006, **96**, 93–101.
- 17 J. Li, X. Y. Li, G. Q. Zhou, W. Wang, C. W. Wang, S. Komarneni and Y. J. Wang, *Appl. Catal., A*, 2014, **470**, 115–122.
- 18 A. Q. Zheng, Z. L. Zhao, S. Chang, Z. Huang, H. X. Wu, X. B. Wang, F. He and H. B. Li, *J. Mol. Catal. A: Chem.*, 2014, **383**, 23–30.
- 19 J. Jae, G. A. Tompsett, A. J. Foster, K. D. Hammond, S. M. Auerbach, R. F. Lobo and G. W. Huber, *J. Catal.*, 2011, **279**, 257–268.
- 20 D. J. Mihalcik, C. A. Mullen and A. A. Boateng, *J. Anal. Appl. Pyrolysis*, 2011, **92**, 224–232.
- 21 G. T. Neumann and J. C. Hicks, *ACS Catal.*, 2012, **2**, 642–646.
- 22 E. F. Iliopoulou, S. Stefanidis, K. Kalogiannis, A. C. Psarras, A. Delimitis, K. S. Triantafyllidis and A. A. Lappas, *Green Chem.*, 2014, **16**, 662–674.
- 23 A. Pattiya, J. O. Titiloye and A. V. Bridgwater, *Fuel*, 2010, **89**, 244–253.
- 24 S. C. Du, Y. J. Sun, D. P. Gamliel, J. A. Valla and G. M. Bollas, *Bioresour. Technol.*, 2014, **169**, 188–197.
- 25 H. Y. Zhang, T. R. Carlson, R. Xiao and G. W. Huber, *Green Chem.*, 2012, **14**, 98–110.
- 26 K. G. Wang and R. C. Brown, *Green Chem.*, 2013, **15**, 675–681.
- 27 P. R. Patwardhan, J. A. Satrio, R. C. Brown and B. H. Shanks, *Bioresour. Technol.*, 2010, **101**, 4646–4655.
- 28 C. A. Mullen and A. A. Boateng, *Ind. Eng. Chem. Res.*, 2013, **52**, 17156–17161.
- 29 C. A. Mullen, A. A. Boateng, R. B. Dadson and F. M. Hashem, *Energy Fuels*, 2014, **28**, 7014–7024.
- 30 H. P. Yang, R. Yan, H. P. Chen, D. H. Lee and C. G. Zheng, *Fuel*, 2007, **86**, 1781–1788.
- 31 S. L. Du, H. P. Yang, K. Z. Qian, X. H. Wang and H. P. Chen, *Fuel*, 2014, **117**, 1281–1287.
- 32 Q. Zhang, J. Chang, T. J. Wang and Y. Xu, *Energy Convers Manage*, 2007, **48**, 87–92.
- 33 E. Kantarelis, W. H. Yang and W. Blasiak, *Energy Fuels*, 2013, **27**, 4748–4759.
- 34 P. T. Williams, N. Nugranad and P. A. Horne, *Biomass Gasification and Pyrolysis: State of the Art and Future Prospects*, 1997, 422–430.
- 35 C. Gilbert, J. Espindola, W. Conner, J. O. Trierweiler and G. W. Huber, *ChemCatChem*, 2014, **6**, 2497–2500.
- 36 E. F. Iliopoulou, E. V. Antonakou, S. A. Karakoulia, I. A. Vasalos, A. A. Lappas and K. S. Triantafyllidis, *Chem. Eng. J.*, 2007, **134**, 51–57.
- 37 L. H. Ong, M. Domok, R. Olindo, A. C. van Veen and J. A. Lercher, *Microporous Mesoporous Mater.*, 2012, **164**, 9–20.
- 38 A. Corma, J. Mengual and P. J. Miguel, *Appl. Catal., A*, 2012, **417**, 220–235.

- 39 A. Corma, O. Marie and F. J. Ortega, *J. Catal.*, 2004, **222**, 338–347.
- 40 A. Corma, J. Mengual and P. J. Miguel, *Appl. Catal., A*, 2012, **421**, 121–134.
- 41 Y. J. Lee, J. M. Kim, J. W. Bae, C. H. Shin and K. W. Jun, *Fuel*, 2009, **88**, 1915–1921.
- 42 D. S. Shihabi, W. E. Garwood, P. Chu, J. N. Miale, R. M. Lago, C. T. W. Chu and C. D. Chang, *J. Catal.*, 1985, **93**, 471–474.
- 43 J. M. Fougerit, N. S. Gnep, M. Guisnet, P. Amigues, J. L. Duplan and F. Hugues, *Zeolites and Related Microporous Materials: State of the Art 1994*, 1994, **84**, 1723–1730.
- 44 E. Kantarelis, W. Yang and W. Blasiak, *Fuel*, 2014, **122**, 119–125.
- 45 T. Blasco, A. Corma and J. Martinez-Triguero, *J. Catal.*, 2006, **237**, 267–277.
- 46 C. Baerlocher, W. M. Meier and D. Olson, *Atlas of zeolite framework types*, Elsevier, Amsterdam, New York, 2007.
- 47 S. H. Jhung, J. S. Chang, J. S. Hwang and S. E. Park, *Microporous Mesoporous Mater.*, 2003, **64**, 33–39.
- 48 K. Barbera, F. Bonino, S. Bordiga, T. V. W. Janssens and P. Beato, *J. Catal.*, 2011, **280**, 196–205.
- 49 P. Ratnasamy, G. P. Babu, A. J. Chandwadkar and S. B. Kulkarni, *Zeolites*, 1986, **6**, 98–100.
- 50 S. K. Sahoo, N. Viswanadham, N. Ray, J. K. Gupta and I. D. Singh, *Appl. Catal., A*, 2001, **205**, 1–10.
- 51 K. S. W. Sing, D. H. Everett, R. A. W. Haul, L. Moscou, R. A. Pierotti, J. Rouquerol and T. Siemieniewska, *Pure Appl. Chem.*, 1985, **57**, 603–619.
- 52 N. Viswanadham, G. M. Dhar and T. S. R. P. Rao, *J. Mol. Catal. A: Chem.*, 1997, **125**, L87–L90.
- 53 N. Viswanadham, R. Kamble, M. Singh, M. Kumar and G. M. Dhar, *Catal. Today*, 2009, **141**, 182–186.